

# An Improved Compliance Model on Meshing Stiffness of Spur Gear Pair by Generating Method of Rack Cutter with Various Gear Parameters

Chuen-Ren Wang\*, Ting-Nung Shiau\*\*, Kuo-Hsuan Huang\*\*\*, De-Shin Liu\*\* and Wei-Chun Hsu\*\*\*\*

**Keywords:** Gear body deflection, Non-constant Hertzian contact, Rack cutter, Generating method.

## ABSTRACT

This study proposes an improved compliance model for the mesh stiffness of a spur gear pair with the various gear parameters. The first step of the proposed model is to use the generating method of rack cutter to obtain an involute tooth profile. The second step is to calculate the mesh stiffness of a gear pair, using gear body deflection of involute tooth with the effects of circular elastic rings under dedendum circle and non-constant Hertzian contact theory. Numerical results show that the magnitude of gear mesh stiffness for the proposed model is of about 20% differences compared to Weber's model and Sianaot's model. It implies that the proposed model can avoid the overestimate problem of gear mesh stiffness. Furthermore, the variations of gear mesh stiffness for the various gear tooth types will affect the system more than the various pressure angles under the non-constant Hertzian contact effect.

## 1. INTRODUCTION

In power transmission the driving gear is always equipped with motor which transmits required torque to the driven gear. Generally speaking, the engaged

procedure of the driving gear and the driven gear can divide into a single-tooth or the multi-teeth engagement. The involute tooth profile was mostly established from the computer-aided design software in the published references. However, there are obstacles and lack of efficiency in order to obtain the involute tooth profile of spur gear by user's specification.

Many researchers have developed analytical methods to study the gear mesh stiffness of a gear pair under the sinusoidal function or Fourier series expansion. The fluctuation of gear mesh stiffness regarded as a periodic excitation was early used by Harris (1958). Kahraman et al. (1996) investigated analytically steady state forced response of a gear system by using the periodic gear mesh stiffness. The influence of involute contact ratio (ICR) with the torsional vibration behavior of a spur gear pair based on the measuring experiment of the dynamic transmission error, and periodic rectangular wave function was studied by Kahraman and Blankeship (1999). They explained the relationship between ICR and gear mesh stiffness. Parker et al. (2000) employed the finite element and contact mechanical model with sinusoidal series of gear mesh stiffness, and investigated the dynamic response of a gear pair with backlash. Theodossiades and Natisavas (2001) illustrated the dynamic response of a gear pair with the periodic gear mesh stiffness to discuss the specific parameters under the quasi-periodic motion and chaotic motion. Later, Shen et. al. (2006) used IHBM to analyze the nonlinear dynamics of a spur gear pair including a backlash, type of multi-term Fourier series for gear mesh stiffness and static transmission error. Fourier series formulation of the gear mesh stiffness of gear train with the dynamic backlash was still employed by Chen et al. (2011). The chaotic region of gear train were appeared early due to the dynamic backlash, friction, and meshing stiffness. Similarly, Al-shyyab and Kahraman (2005) employed a multi-term Fourier series to simulate the gear mesh stiffness, and investigated analytically the steady state forced response of a multi-mesh geared system.

The developed model of the compliance model

*Paper Received October 2014. Revised November, 2015, Accepted December, 2015, Author for Correspondence: Chuen-Ren Wang*

*\* Postgraduate, Advanced Institute of Manufacturing with High-tech Innovations and Department of Mechanical Engineering, National Chung Cheng University. 621 Chia-Yi, Taiwan, R.O.C.*

*\*\*Professor, National Chung Cheng University. 621 Chia-Yi, Taiwan, R.O.C.*

*\*\*\* Manager, L. K. Machinery Corp. 407, Taichung.*

*\*\*\*\*Assistant professor, Department of Mechanical Engineering, WuFeng University. 621 Chia-Yi, Taiwan, R.O.C.*

and Hertzian contact for involute gear tooth was firstly followed to Weber (1949), who regarded the compliance of gear tooth as the assembly of basic deflection of the tooth as a beam, the fillet and foundation flexibility, and the local deflection caused by Hertzian contact. Muskhelishvili (1975) presented a general bidimensional solution for circular rings based on a complex power series representation. Then, Cornell (1981) proposed the compliance method from Weber's model to calculate the deflection of involute gear tooth. The theory of parallel connection and curve fitting were further employed to simulate the meshing stiffness of a multi-teeth gear pair. Yang (1985) employed the material compliance and energy dissipation to obtain the gear body deflection. P. Sainaot et al. (2004) proposed an improved model based on the theory of scholar Muskhelishvili. The proposed model was in agreement with FEM model and the formulation was more accurate than that of Weber's model. Kuang et al. (1992,2001) used the quadratic plane-strain element with finite element method to disperse the continuous gear body, and substituted for the deflection results of gear to obtain the meshing stiffness by curve fitting. Chaari et al. (2008) considered the effect of spalling or tooth breakage on the procedure of gear mesh stiffness for a one-stage spur gear transmission. The width of breakage affected obviously in decreasing the gear mesh stiffness. Next year, Chaari et al. (2009) illustrated the crack effect on the gear mesh stiffness of a gear pair. The gear mesh stiffness reduction was accentuated by large crack inclination angle as depth of crack increased.

The undercutting analysis for developed mathematical model of elliptical model based on the theory of gearing and the geometry of the straight-sided rack cutter are illustrated with Chang et al. (1994). This model was included the fillets, working regions, top land and backlash. Litvin (2004) later explained the mathematical model of planer, helical elliptical, involute gear, and introduced the theory of the equation of meshing for generating method of various gear. Litvin et al. (2007) proposed the generation of planer and helical elliptical gears to be employed in application of rack-cutter, hob, and shaper. Chen et al. (2011) used the energy storage theory of bending, shear and axial compression to simulate the deflection of a spur gear as a non-uniform cantilever beam. In last three years, the gear mesh stiffness subjected to the influence of crack is certain to carry weight. Ma and Chen (2012) used the 3D FE model to obtain the gear mesh stiffness and load sharing ratio. On the basis of Ref. (2004,2008,2009), Mohammed et al. (2013), Wan et al. (2014), Ma et al. (2014) used the compliance algorithm and energy method to obtain the gear mesh stiffness with the crack effect.

The multi-term Fourier series expansion or the rectangular wave function was conveniently assigned to approximate the gear mesh stiffness, but above simulation model could not exhibited the realistic engaged procedure. Focusing on these problems, the

proposed model of this paper adopts the generating method of rack cutter to create the involute gear tooth profile. Further, the circular elastic rings under dedendum circle and non-constant Hertzian contact theory is considered at the improved compliance model to calculate the gear body deflection.

## 2. Generation of Rack Cutter and Gear mesh Stiffness

The rectangular wave function or Fourier series expansion were used to approximate the gear mesh stiffness of a gear pair at mostly previous paper. A few papers (1949, 1981, 2008, 2009) was used the compliance methodology to calculate the gear mesh stiffness of a single gear pair. This paper summarizes the advantages of published papers to propose the improved mathematical model of compliance methodology. The proposed methodology can be applied to obtain rapidly the involute tooth of spur gear due to the generating method of rack cutter.

### 2.1 Mathematical model of rack cutter

The mathematic model of rack cutter consists of straight line and arc as shown in Fig.1 (a). The mathematic model of rack cutter can be expressed as

$$\mathbf{r}_2^{(1)} = \begin{bmatrix} \mp(u_1 \sin \alpha - t_f \tan \alpha - t_0 / 2) \\ u_1 \cos \alpha - t_f \\ 1 \end{bmatrix} \quad (1)$$

$$\mathbf{r}_2^{(2)} = \begin{bmatrix} \pm(t_0 / 2 - t_f \tan \alpha - \rho \cos \alpha - \rho \cos \theta_1) \\ -t_f + \rho \sin \alpha + \rho \sin \theta_1 \\ 1 \end{bmatrix}$$

Where, superscript (1) and (2) are the straight line and arc, respectively. Subscript indicates the vector of rack cutter in the coordinate of  $S_f$ . The "+" and "-" denote the right and left hand side of a rack cutter model, respectively.

Coordinate system of  $S_f$  and  $S_2$  are rigidly connected to a gear pair, and are performed the translational and rotational motions with respect to the fixed coordinate system. In other words, the trajectory of rack cutter must be described the motion of rack cutter at rotational coordinate. As show in Fig.1 (b),  $S_f$ ,  $S_f$ ,  $S_2$  denote the fixed coordinate, the horizontal moving coordinate of rack cutter, and the rotational coordinate of gear. The vector  $\mathbf{r}_2$  of rack cutter at rotational coordinate  $S_2$  can be given by

$$\mathbf{r}_2^{(1)} = [M_{21}] \mathbf{r}_1^{(1)}, \quad \mathbf{r}_2^{(2)} = [M_{21}] \mathbf{r}_1^{(2)} \quad (2)$$

Transformation coordinate from  $S_f$  to  $S_2$  is illustrated with the Eqns. (3) and (4). The transformation matrix of  $M_{21}$  means that the translational coordinate of  $S_f$  transfers to the rotational coordinate of  $S_2$ . The transformation matrix are expressed as

$$[M_{21}] = [M_{2f}] [M_{f1}] \quad (3)$$

$$[M_{2f}] = \begin{bmatrix} \cos \phi & \sin \phi & 0 \\ -\sin \phi & \cos \phi & 0 \\ 0 & 0 & 1 \end{bmatrix}, [M_{f1}] = \begin{bmatrix} 1 & 0 & -r_o \phi \\ 0 & 1 & r_o \\ 0 & 0 & 1 \end{bmatrix}$$

$$[M_{21}] = \begin{bmatrix} \cos \phi & \sin \phi & r_o(\sin \phi - \phi \cos \phi) \\ -\sin \phi & \cos \phi & r_o(\cos \phi + \phi \sin \phi) \\ 0 & 0 & 1 \end{bmatrix} \quad (4)$$

Where  $r_o$  is radius of base circle and  $\phi$  is rotational angle. According to the Eqns. (2), (3), and (4), the vector of rack cutter at the rotational coordinate of  $S_2$  is given by

$$\mathbf{r}_2^{(1)} = \begin{bmatrix} \sin \phi(-t_f + u_1 \cos \alpha) + r_o(\sin \phi - \phi \cos \phi) \pm \\ (\cos \phi(\frac{t_0}{2} + u_1 \sin \alpha - t_f \tan \alpha)) \\ \cos \phi(-t_f + u_1 \cos \alpha) + r_o(\cos \phi + \phi \sin \phi) \pm \\ (-\sin \phi(\frac{t_0}{2} + u_1 \sin \alpha - t_f \tan \alpha)) \\ 1 \end{bmatrix}$$

$$\mathbf{r}_2^{(2)} = \begin{bmatrix} \sin \phi(\rho \sin \alpha + \rho \sin \theta_1 - t_f) + r_o(\sin \phi - \phi \cos \phi) \pm \\ (\cos \phi(-\rho \cos \alpha - \rho \cos \theta_1 + \frac{t_0}{2} - t_f \tan \alpha)) \\ \cos \phi(\rho \sin \alpha + \rho \sin \theta_1 - t_f) + r_o(\cos \phi + \phi \sin \phi) \pm \\ (-\sin \phi(-\rho \cos \alpha - \rho \cos \theta_1 + \frac{t_0}{2} - t_f \tan \alpha)) \\ 1 \end{bmatrix} \quad (5)$$

Where  $h_f$  is addendum,  $t_f$  is dedendum,  $u_1$  is the line section of rack cutter,  $t_0$  is standard pitch,  $\rho$  is radius of fillet,  $\theta_1$  is angle of arc section of rack cutter,  $\alpha$  is pressure angle. The vector of rack cutter is function of  $u_1, \theta$ , and  $\phi$ , respectively, as shown in Eqns. (5). The trajectory of rack cutter can be drew tooth profile with the envelope of generating method when rotational angle of  $\phi$  increase gradually. The every point on the envelope of rack cutter is solved by equation of meshing. Consequently, the involute tooth profile of spur gear can be constituted by the summation of those points.

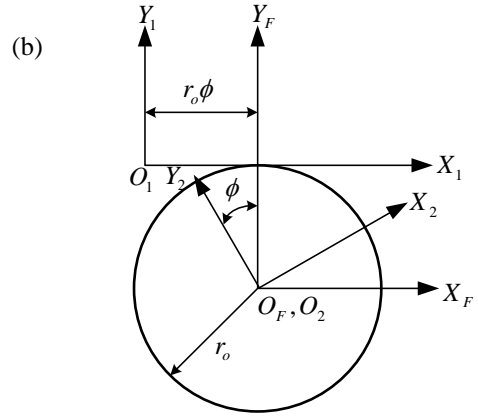
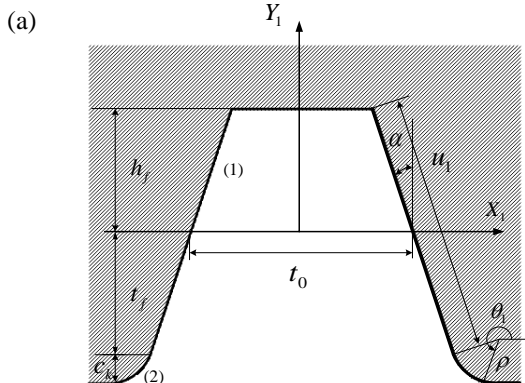


Fig. 1. The mathematic model of rack cutter and coordinate of  $S_F, S_1, S_2$

According to the principle of equation of meshing, the tangent vector  $\mathbf{V}^{(12)}$  and normal vector  $\mathbf{N}$  are orthogonal to each other on the tooth surface. The formulation can be expressed as

$$\mathbf{N} \cdot \mathbf{V}^{(12)} = 0 \quad (6)$$

According to the Eqn. (6), the necessary condition of envelope are given by

$$f^{(1)}(u_1, \phi) = \left( \frac{\partial \mathbf{r}_2^{(1)}(u_1, \phi)}{\partial u_1} \times \bar{k} \right) \cdot \frac{\partial \mathbf{r}_2^{(1)}(u_1, \phi)}{\partial \phi} = 0$$

$$f^{(2)}(\theta, \phi) = \left( \frac{\partial \mathbf{r}_2^{(1)}(\theta, \phi)}{\partial \theta} \times \bar{k} \right) \cdot \frac{\partial \mathbf{r}_2^{(1)}(\theta, \phi)}{\partial \phi} = 0 \quad (7)$$

And the normal vector of the tooth surface of spur gear are defined as

$$\mathbf{N}_2^{(1)} = \frac{\partial \mathbf{r}_2^{(1)}}{\partial u_1} \times \bar{k}$$

$$\mathbf{N}_2^{(2)} = \frac{\partial \mathbf{r}_2^{(2)}}{\partial \theta} \times \bar{k} \quad (8)$$

The vector of tooth profile of  $\mathbf{r}$  and dimensionless normal vector of  $\mathbf{n}$  at the rotating coordinate of  $S_2$  are respectively given by the Eqns.(2), (5) and (7).

$$\mathbf{r}_2^{(1)} = \begin{bmatrix} \pm(-r_o \sin a_1 + b_1 \cos(a_1 - \alpha)) \\ r_o \cos a_1 + b_1 \sin(a_1 - \alpha) \\ 1 \end{bmatrix}$$

$$\mathbf{r}_2^{(2)} = \begin{bmatrix} \pm(-r_o \sin a_2 + b_2 \cos(a_2 - \theta_1)) \\ r_o \cos a_2 + b_2 \sin(a_2 - \theta_1) \\ 1 \end{bmatrix} \quad (9)$$

$$\mathbf{n}_2^{(1)} = \frac{\mathbf{N}_2^{(1)}}{|\mathbf{N}_2^{(1)}|} = [\cos(a_2 - \alpha) \quad \mp \sin(a_2 - \alpha) \quad 0]^T$$

$$\mathbf{n}_2^{(2)} = \frac{\mathbf{N}_2^{(2)}}{|\mathbf{N}_2^{(2)}|} = [\cos(b_2 - \alpha) \quad \mp \sin(b_2 - \alpha) \quad 0]^T \quad (10)$$

Here,

$$a_1 = \frac{t_0 + 2t_f \csc \alpha \sec \alpha - 2u_1 \csc \alpha}{2r_o}$$

$$a_2 = \frac{t_0 + 2(\rho(\cos \alpha - \cot \theta_1 \sin \alpha) + t_f(\cot \theta_1 + \tan \alpha))}{2r_o}$$
(11)

$$b_1 = \csc \alpha(t_f - u_1 \cos \alpha)$$

$$b_2 = \rho + \rho \csc \theta_1 \sin \alpha - t_f \csc \theta_1$$
(12)

The vector of tooth profile of  $r_{2g}$  and  $r_{2p}$  are calculated by Eqn. (9). Consequently, the transformation matrix and unit normal vector for vector of tooth profile must be transformed from rotational coordinate  $S_2$  to fixed coordinate  $S_F$ . Those matrices are expressed as

$$r_{Fp}^{(1)} = [M_{Fp}] r_p^{(1)}, r_{Fg}^{(1)} = [M_{Fg}] r_g^{(1)}$$
(13)

$$n_{Fp}^{(1)} = [L_{Fp}] n_p^{(1)}, n_{Fg}^{(1)} = [L_{Fg}] n_g^{(1)}$$
(14)

$$[M_{Fp}] = \begin{bmatrix} \cos \phi_p & -\sin \phi_p & 0 \\ \sin \phi_p & \cos \phi_p & -c_p \\ 0 & 0 & 1 \end{bmatrix}$$
(15)

$$[M_{Fg}] = \begin{bmatrix} \cos \phi_g & \sin \phi_g & 0 \\ -\sin \phi_g & \cos \phi_g & r_{op} + r_{og} + c_g \\ 0 & 0 & 1 \end{bmatrix}$$

$$[L_{Fp}] = \begin{bmatrix} \cos \phi_p & -\sin \phi_p \\ \sin \phi_p & \cos \phi_p \end{bmatrix}, [L_{Fg}] = \begin{bmatrix} \cos \phi_g & \sin \phi_g \\ -\sin \phi_g & \cos \phi_g \end{bmatrix}$$
(16)

Where  $\phi_p$  and  $\phi_g$  are rotational angle of pinion and gear.  $c_p$  and  $c_g$  are offset distance of pinion and gear.  $r_{op}$  and  $r_{og}$  are radii of pitch circles for pinion and gear, respectively. The tooth vectors of gear and pinion and unit normal vector are given by Eqns. (17), (18) and (19).

$$r_{Fp}^{(1)} = \begin{bmatrix} \pm(-r_p \sin(a_1 \pm \phi_p) + b_1 \cos(a_1 - \alpha \pm \phi_p)) \\ r_p \cos(a_1 \pm \phi_p) + b_1 \cos(a_1 - \alpha \pm \phi_p) - c_p \\ 1 \end{bmatrix}$$
(17)

$$r_{Fg}^{(1)} = \begin{bmatrix} \pm(-r_g \sin(a_1 \pm \phi_g) + b_1 \cos(a_1 - \alpha \pm (-\phi_g))) \\ 2r_g \cos(\frac{a_1 \pm (-\phi_g)}{2})^2 + b_1 \sin(a_1 - \alpha \pm (-\phi_g)) + r_p + c_g \\ 1 \end{bmatrix}$$
(18)

$$n_{Fp}^{(1)} = \begin{bmatrix} \cos(a_1 - \alpha \pm \phi_p) \\ \pm \sin(a_1 - \alpha \pm \phi_p) \end{bmatrix}, n_{Fg}^{(1)} = \begin{bmatrix} \cos(a_1 - \alpha \pm \phi_g) \\ \pm \sin(a_1 - \alpha \pm \phi_g) \end{bmatrix}$$
(19)

Similarly, the position of meshing point on the pitch circle is obtained by employing the equation of meshing. There are three equations and four unknown quantities in Eqn. (20) and Eqn. (21), respectively.

Consequently, the position of any points along the line of action can be obtained if rotational angle of pinion is given.

$$r_{Fp}^{(1)} - r_{Fg}^{(1)} = 0, n_{Fp}^{(1)} - n_{Fg}^{(1)} = 0$$
(20)

$$|n_{Fp}^{(1)}| = |n_{Fg}^{(1)}| = 1$$
(21)

## 2.2 Compliance methodology

The concept of gear tooth compliance is cited from Weber (1949) which is introduced to make up three subsections. They are the basic tooth as a cantilever beam, fillet-foundation deflection and Hertzian contact, respectively. The compliance of involute tooth subjected to the normal force due to the applied force can be given as follow.

$$C = y_T / F_L$$
(22)

$$y_T = (y_{Bp} + y_{Fp}) + (y_{Bg} + y_{Fg}) + y_L$$
(23)

Where  $y_T$  is total deflection,  $F_L$  is applied force.

$y_{Bp}$  and  $y_{Bg}$  are regarded tooth deflections of the pinion and gear as a cantilever beam due to bending moment, respectively.

### 2.2.1 Gear tooth deflection

The tooth deflection of pinion and gear are regarded as cantilever beam by Weber (1949) as shown in Fig. (2a). The formulation of deflection for plane stress and plane strain are given by

For plane stress,

$$y_{Bg} = y_{Bp} = \frac{F_L \cos^2 \alpha'_{bp}}{E} \sum_{i=1}^k \delta_i \left[ \frac{(l_i^2 - l_i \delta_i + \frac{1}{3} \delta_i^2)}{\bar{I}_i} + \frac{(2.4(1 + \mu) + \tan^2 \alpha'_{bp})}{\bar{A}_i} \right]$$
(24)

For plane strain,

$$y_{Bg} = y_{Bp} = \frac{F_L \cos^2 \alpha'_{bp}}{E} \sum_{i=1}^k \delta_i \left[ \frac{(l_i^2 - l_i \delta_i + \frac{1}{3} \delta_i^2)(1 - \mu^2)}{\bar{I}_i} + \frac{(2.4(1 + \mu) + \tan^2 \alpha'_{bp})}{\bar{A}_i} \right]$$
(25)

Where  $k$  is number of element,  $E$  is Young's modulus, and  $\mu$  is Poisson's ratio.  $h_F$  is length of tooth base which is defined as  $h_F = 2r_{px1}^{(1)}$ . The distance of applied load from base is  $l_F = r_{pLy}^{(1)} - r_{py1}^{(2)}$ . The moment of mass inertia for each element  $I_i$  is  $W \cdot (2r_{pxi})^3 / 12$ .  $W$  and  $r_{pxi}$  are width of gear and  $x$  coordinate of  $i$ -th element, respectively. The cross-section area is  $A_i = W \cdot (2r_{pxi})$ . The moment of inertia of area and the cross-section area are expressed as  $1/\bar{I}_i = (1/I_i + 1/I_{i+1})/2$  and  $1/\bar{A}_i = (1/A_i + 1/A_{i+1})/2$ , respectively. The magnitude of element of load ( $l_i$ ),

width of element ( $\delta_i$ ) and angle of applied load ( $\alpha'_{bp}$ ) in Eqn. (24) and Eqn. (25) are expressed as  $l_i = r_{pLy} - r_{pyi}$ ,  $\delta_i = r_{pyi+1} - r_{pyi}$ ,  $\alpha'_{bp} = \alpha_b - \alpha_{Lp}$ , respectively.

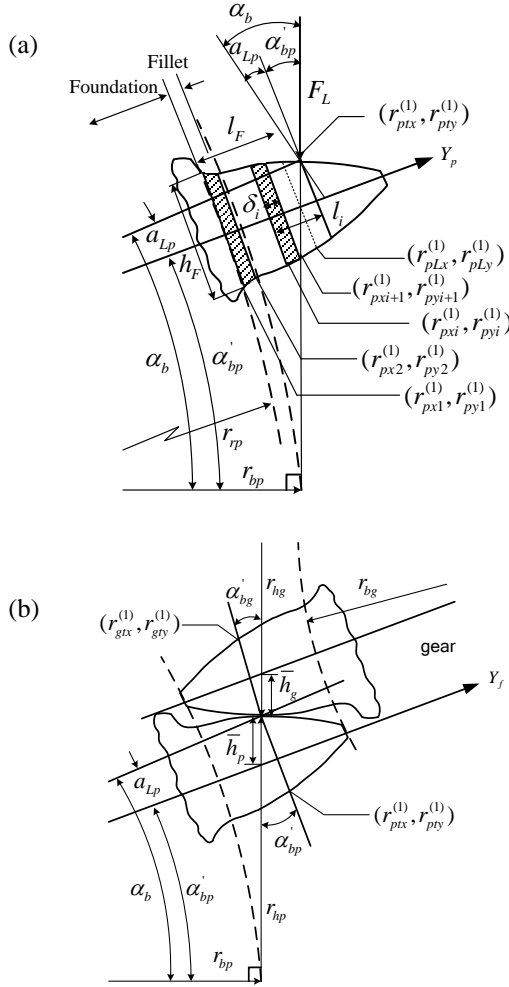


Fig. 2. (a) Beam, fillet and foundation compliance of a gear tooth (b) Hertz contact of a gear tooth.

### 2.2.2 Fillet-foundation deflection

The models of Cornell and Sainot are similar and they consider the deflection of fillet-foundation. However, the assumption of circular elastic rings under the dedendum circle by Sainot is different from fillet-foundation by Cornell. Cornell regarded the fillet as flexible material to create the additional deflection with load. The deflection direction of tooth with load is based on the foundation effect of  $y_{fp}$  as shown in Fig. (3a).

For plane stress,

$$y_{fp} = y_{fg} = \frac{F_L \cos^2 \alpha'_{bp}}{WE} \left[ \frac{16.67}{\pi} \left( \frac{l_F}{h_F} \right)^2 + 2(1-\mu) \left( \frac{l_F}{h_F} \right) + 1.534 \left( 1 + \frac{\tan^2 \alpha'_{bp}}{2.4(1+\mu)} \right) \right] \quad (26-1)$$

For plane strain,

$$y_{fp} = y_{fg} = \frac{F_L \cos^2 \alpha'_{bp}}{WE} (1-\mu^2) \left[ \frac{16.67}{\pi} \left( \frac{l_F}{h_F} \right)^2 + 2 \left( \frac{1-\mu-2\mu^2}{1-\mu^2} \right) \left( \frac{l_F}{h_F} \right) + 1.534 \left( 1 + \frac{\tan^2 \alpha'_{bp}}{2.4(1+\mu)} \right) \right] \quad (26-2)$$

Further, the theory of Muskhelishvili and Sainot for fillet-foundation deflection is applied with the circular elastic rings to assume the constant contact stress as shown in Fig. (3b). The analytical expression reflects the gear body-induced tooth deflection by assuming the constant contact stress at the dedendum circle, which is given by

$$y_{fp} = y_{fg} = \frac{F \cos^2 \alpha}{WE} \left\{ L^* \left( \frac{u_f}{S_f} \right)^2 + M^* \left( \frac{u_f}{S_f} \right) + P^* \left( 1 + Q^* \tan^2 \alpha \right) \right\} \quad (27-1)$$

$L^*(h_{fi}, \theta_f)$ ,  $L^*(h_{fi}, \theta_f)$ ,  $L^*(h_{fi}, \theta_f)$  and  $L^*(h_{fi}, \theta_f)$  are limited in ranges of variation ( $h$  between 1.4 and 7,  $\theta_f$  between 0.01 and 0.12) for plane strain. The coefficient  $L^*$ ,  $M^*$ ,  $P^*$ ,  $Q^*$  can be approached by the polynomial function.

$$X_i^* (h_{fi}, \theta_f) = A_i \left( \frac{1}{\theta_f^2} \right) + B_i h_{fi}^2 + C_i \left( \frac{h_{fi}}{\theta_f} \right) + D_i \left( \frac{1}{\theta_f} \right) + E_i h_{fi} + F_i \quad (27-2)$$

Where,  $W$  is tooth width,  $E$  is Young's modulus,  $F$  is applied load,  $u_f, S_f, h_{fi} = r_f / r_{int}$  and  $\theta_f$  are defined in Fig. (3b). Those values of  $A_i, B_i, C_i, D_i, E_i$  and  $F_i$  are given in Table 1.

Table 1. Values of the coefficient of Eq. (27-2)

	$A_i$	$B_i$	$C_i$	$D_i$	$E_i$	$F_i$
$L^*(h_{fi}, \theta_f)$	$-5.574e^{-5}$	$-1.9986e^{-3}$	$-2.3015e^{-4}$	$4.77021e^{-3}$	0.0271	6.8045
$M^*(h_{fi}, \theta_f)$	$60.111e^{-5}$	$28.100e^{-3}$	$-83.431e^{-4}$	$-9.9256e^{-3}$	0.1624	0.9086
$P^*(h_{fi}, \theta_f)$	$-50.952e^{-5}$	$185.50e^{-3}$	$0.0538e^{-4}$	$53.300e^{-3}$	0.2895	0.9236
$Q^*(h_{fi}, \theta_f)$	$-6.2042e^{-5}$	$9.0889e^{-3}$	$-4.0964e^{-4}$	$7.8297e^{-3}$	-0.1472	0.6904

### 2.2.3 Hertzian contact

Hertzian contact theory is comprehensively applied for the contact behavior of both elastic bodies. Here two types of Hertzian theory are introduced to distinguish the differences between Weber's model and Sainot's model. First, Yang (1985) used the constant Hertzian contact at meshing condition along the line of action. The local compression  $y_L$  is given by

$$y_L = F_L \left[ \frac{4(1-\mu^2)}{\pi WE} \right] \quad (28)$$

Hertzian contact is non-constant along the line of action in the physical phenomenon of meshing situation. Consequently, this study refers that the Weber's model can improve the theory of Yang's model. As shown in Fig. (2b), the local compression of each tooth between the contact point and tooth centerline is approximated by assuming the load spread at a various

meshing pressure angle. The local compliance of  $y'_L$  is assumed to increase linearly with  $L/W$ . The expression of compliance from Muskhelishvili (1975) without the contact width effect is given by

$$y'_L \approx 3.57 \left[ \frac{4F_L(1-\mu^2)}{\pi WE} \right] \quad (29-1)$$

Similarly, the compliance with the effect of contact width is considered as

$$y'_L = \frac{4F_L(1-\mu^2)}{\pi WE} \left[ \ln \left( \frac{\sqrt{\bar{h}_p \bar{h}_g}}{b_h} \right) - \frac{\mu}{2(1-\mu)} \right] \quad (29-2)$$

Here,

$$b_h = \left[ \frac{8F_L(1-\mu^2)}{\pi WE} \right] / \left( \frac{1}{r_{hp}} + \frac{1}{r_{hg}} \right) \quad (30)$$

$$r_{hp} = r_{bp} \tan \alpha_b, \quad r_{hg} = r_{bg} \tan \alpha_b \quad (31)$$

$$\bar{h}_p = r_{pix}^{(1)} / \cos \alpha'_{bp}, \quad \bar{h}_g = r_{gix}^{(1)} / \cos \alpha'_{bg} \quad (32)$$

The  $r_{bp}$  and  $r_{bg}$  are radii of base circles for pinion and gear, respectively.  $b_h$  is half width of Hertzian contact.  $r_{pix}^{(1)}$  and  $r_{gix}^{(1)}$  are elements of pinion and gear of involute tooth at  $x$  coordinate.  $\alpha'_{bp}$  and  $\alpha'_{bg}$  are meshing pressure angle with mesh point between pinion and gear. Furthermore, Hertzian contact of compliance methodology in this paper is adopted by Eqn. (29-2) to simulate the non-constant Hertzian contact of the engagement.

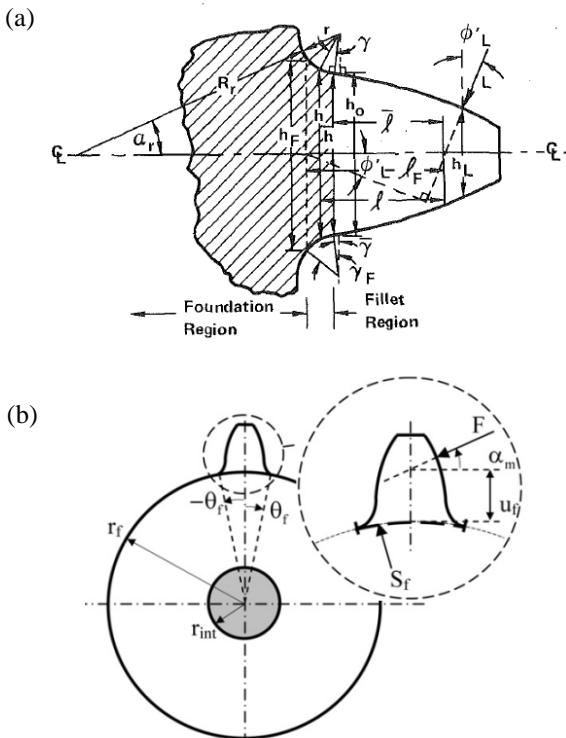


Fig. 3. The geometric of the fillet-foundation deflection comparison of (a) Cornell's model and (b) Sainat's model

### 2.2.4 Meshing stiffness

According to the Eqns. (24), (25), (26)/(27) and (28)/(29), the gear mesh stiffness is computed by summation of deflections for a single gear tooth along point by point. The realistic phenomenon of a meshing condition is either single-tooth engagement or multi-teeth engagement. Consequently, Fig. (4b) show the stiffness of multi-teeth engagement is employed from the parallel connection theory of springs to simulate the gear mesh stiffness. The formulation of gear mesh stiffness of multi-teeth engagement versus the contact ratio are defined as

$$K_m(\bar{\tau}) = \begin{cases} \bar{K}_m(\varepsilon_a) + \bar{K}_m(1 + \varepsilon_a) & 0 \leq \varepsilon_a \leq n \\ \bar{K}_m(\varepsilon_a) & n < \varepsilon_a < (\varepsilon_a - n) \\ \bar{K}_m(\varepsilon_a) + \bar{K}_m(\varepsilon_a - 1) & (\varepsilon_a - n) \leq \varepsilon_a \leq \varepsilon_o \end{cases} \quad (33)$$

Where,  $\varepsilon_a(\bar{\tau})$  is the indiscriminate contact ratio that is represented as  $\varepsilon_a(\bar{\tau}) = s_a(\bar{\tau}) / t_e$ ,  $t_e$  is base pitch, the indiscriminate length on contact length are defined as

$$s_a(\bar{\tau}) = \frac{\phi_{pa} \varepsilon_o}{\phi_{pe} - \phi_{ps}} \quad (34)$$

Here,  $\varepsilon_o$  is contact length at line of action.  $\phi_{ps}$  and  $\phi_{pe}$  are starting contact angle and separable angle of pinion.  $\phi_{pa}$  represents the angle of relative meshing position by subtracting separable angle  $\phi_{pe}$ . The relationship of  $\phi_{pa}$  with time can be presented as

$$\phi_{pa} = \text{mod}((\phi_{p0} + \omega_p) / (\phi_{pe} - \phi_{ps})) \quad (35)$$

The symbol mod represents remainder the of  $(\phi_{p0} + \omega_p) / (\phi_{pe} - \phi_{ps})$ .  $\phi_{p0}$  is initial mesh angle of pinion, and  $\omega_p$  is angular velocity of pinion.

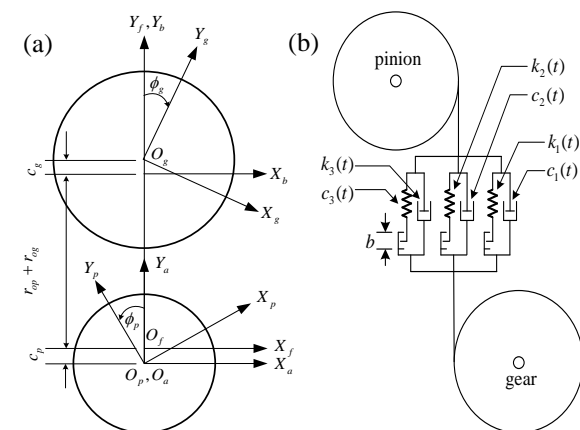


Fig. 4. (a) The corresponding coordinate between the gear and pinion. (b) Parallel model of Multi-tooth mesh stiffness.

### 3. Results and discussion

The circular elastic rings under dedendum circle and non-constant Hertzian contact are considered to simulate the gear mesh stiffness of a spur gear pair in

this paper. To validate the program reliability, the deflections of the spur gear by ANSYS® Workbench 14.0 are compared with those of MATLAB® R2010a. The analytical results are in agreement with Weber's results (1949) as shown in Fig. (5a) and Fig. (5b). Figure (5a) is the solid body of involute spur gear tooth, and Fig (5b) is the comparison of both results of ANSYS® and MATLAB®. The relative error of each other is smaller than 0.5%. Similarly, figure 6 is the comparison of gear mesh stiffness for a spur gear pair between the proposed model and Chaari's model (2001). The numerical results of the proposed model are also in agreement with Chaari's results to validate the accuracy of program.

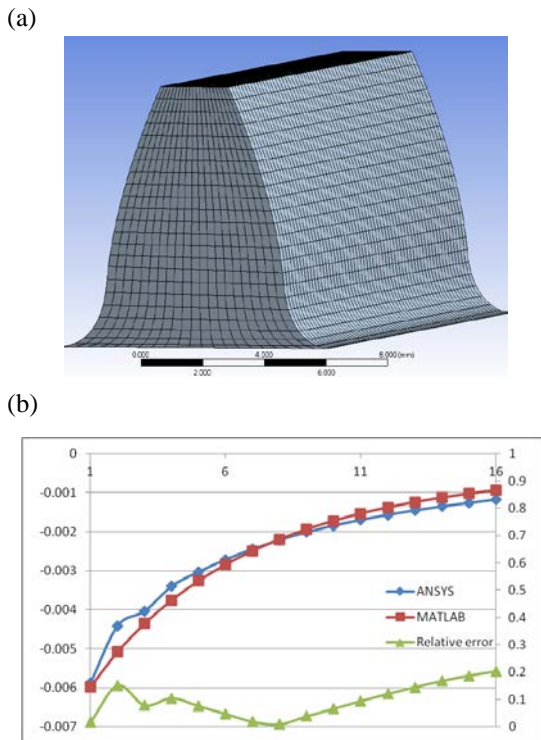


Fig. 5. The (a) tooth profile and (b) deflection results of involute spur gear are simulated by MATLAB® R2010a and ANSYS® Workbench 14.0.

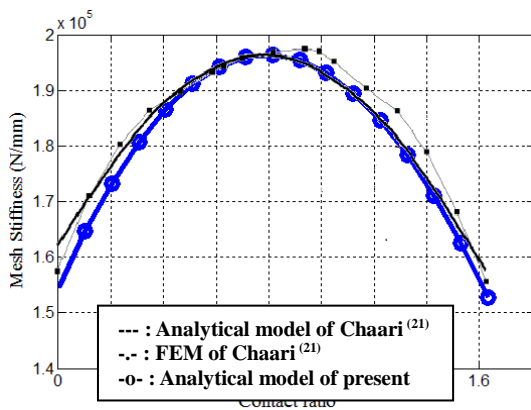


Fig. 6. The gear mesh stiffness of a spur gear pair compared with Chaari's model (2001) and proposed model.

Figure (7a) describes a trajectory of the generation of

rack cutter. The envelope of the trajectory can be observed the prototype of the involute tooth profile of the spur gear. Subsequently, the various types of involute gear tooth, which include stub-tooth, full-tooth and long-tooth, can be created by the generating method of rack cutter, respectively, as shown in Fig. (7b). The time consumptions for the generating method and simulation for the various involute tooth profiles are listed in table 2.

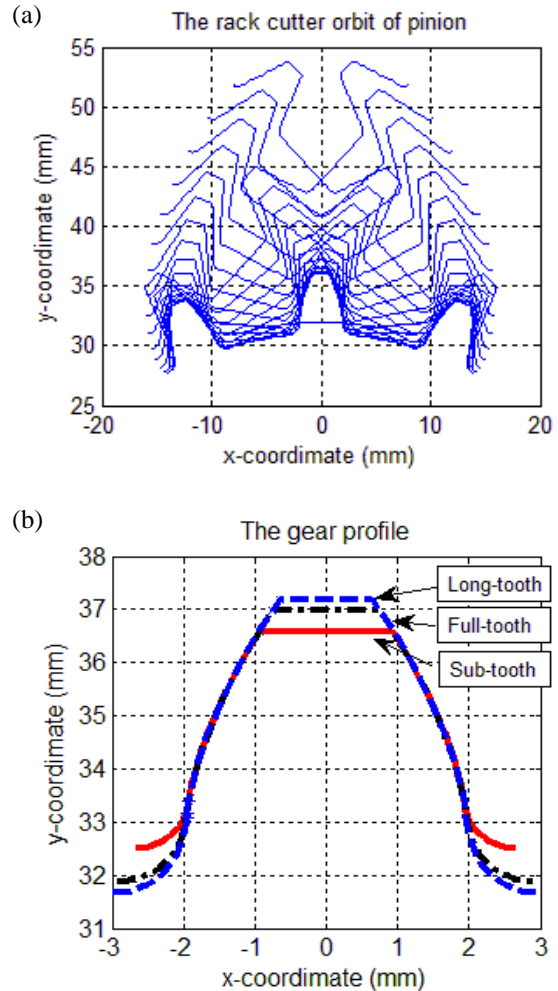


Fig.7. (a) The trajectory of the generating method of rack cutter (b) Tooth types are created by the generating method of rack cutter with various gear parameters.

The circular elastic rings under dedendum circle and defined a back ratio of the circular elastic ring are considered in Sainat's model. Consequently, the description of the gear tooth deflection is better than the fillet-foundation effect of Weber's model. However, Sainat's model regarded Hertzian contact as constant in the engaged procedure. According to the above crucial points, Hertzian contact must include the effect of contact width and load position from Weber's model and the foundation deflection of tooth must consider the circular elastic rings under dedendum circle from Sainat's model. The both advantages are adopted in the proposed model. Consequently, the proposed model

consists of Eqn. (24), (25), (27-1), (27-2) and (29-2), respectively. Furthermore, the specific parameters of the involute spur gear tooth and the contact ratios of various gear tooth types are listed in table 3. The back ratio coefficient of the radii of circular elastic rings for gear and pinion are adopted as 4 and 3.3, respectively.

Table 2. The comparison of time consumption is for the generating method and commercial software.

	Generating method	Measurement	Software
Time consumption	30 sec	>> 1 min	>> 1 min

Table 3. The geometry parameters and contact ratio of the various involute spur gear tooth.

	Stub-tooth gear	Full-tooth gear	Long-tooth gear
Pressure angle( $\alpha$ )	$20^\circ$	Num. of teeth(z) 34,35	
Backlash( $C_b$ )	$0 \mu\text{m}$	Width of tooth(W) 23	
Elastic modulus(E)	$2.0 \times 10^5 \text{ N/mm}^2$	Poisson's ratio( $\nu$ ) 0.3	
Torque(T)	28.13 N-m	Modulus(m) 2	
Addendum( $h_a$ )	0.8m	1.0m	1.1m
Dedendum( $h_f$ )	1.0m	1.25m	1.35m
Clearance( $c_k$ )	0.2m	0.25m	0.25m
Whole depth( $h$ )	1.8m	2.25m	2.45m
Contact ratio( $\epsilon_0$ )	1.3823	1.6836	1.8296

The total deflection of the spur gear and the gear mesh stiffness versus contact ratio with three compliance model are illustrated in Fig. (8a) and Fig. (8b), respectively. The red line, black dotted line and blue dot-dashed line of Fig. (8a) denote the deflections of compliance model with respect to Weber, Sainat and present, respectively. The line with circle denotes that the pinion deflection subjected to meshing force from start point to separated point on the tooth surface along the line of action. It means that the engaged position is from tooth root to tip. The phenomenon of the gear deflection is just the opposite to pinion as the line with rhombus as described. The line with square denotes the deflection of non-constant Hertzian contact. The deflection of non-constant Hertzian contact is smaller than the tooth deflection because the strain mainly occurs on tooth surface. Finally, the solid line denotes the total deflection of engagement of a single gear pair. Fig (8b) shows the gear mesh stiffness with three compliance modals by including the single-tooth engagement and the multi-teeth engagement. The diagram represents that there is 17.64% of the completed gear mesh periodic circle under the single-tooth engaged procedure. In other words, there is 82.36% of the completed gear mesh periodic circle under the multi-teeth engaged procedure. Consequently, the upper diagram of Fig. (8b) exhibits the overlap of the every single-tooth engagement versus the normalized contact position. As shown is Fig. (8b), the contact ratio is from 0 to 0.65 represents the multi-teeth engaged procedure. Therefore, the contact position of single-teeth engaged procedure is form 0.65 to 1.0. In other words, the interval of contact ratio is from 0 to 1.684 includes one single-tooth and two multi-teeth

engagement which denote the one completed meshing procedure at the line of action.

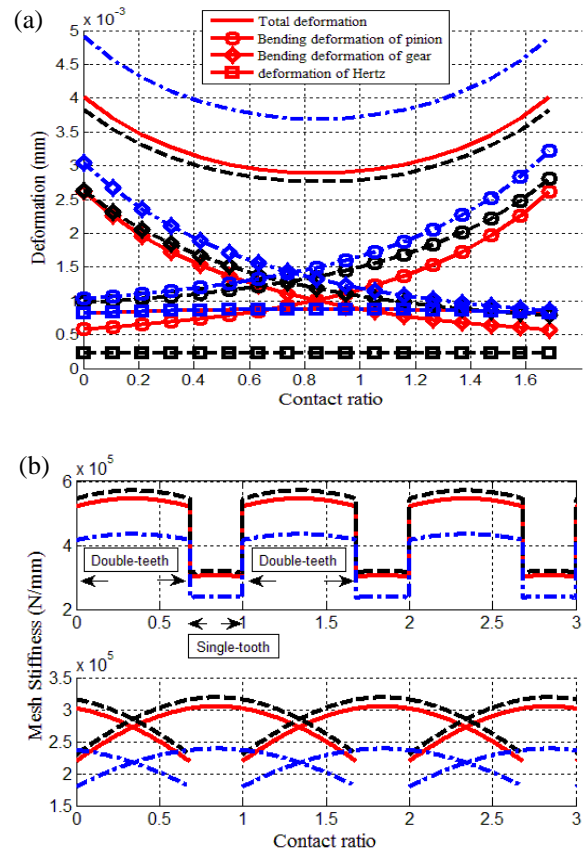


Fig. 8. The total deformation and gear mesh with full-tooth type of the pressure angle of  $20^\circ$  for Weber's model(---), Sainat's model(- -), and Present model(-.-).

Total deflections of the single spur gear pair estimated by Weber's model are similar to those of Sainat's model. However, the results of proposed model are larger than those of both models. It means that the effect of the circular elastic rings under dedendum circle and non-constant Hertzian contact influence the gear body deflection directly. The total deflection of the spur gear can disassemble the individual case to deal with their influences. First, the deflection of the basic tooth regarded as a cantilever beam in Sainat's model is namely similar to that of Weber's model. Second, the circular elastic rings under dedendum circle and the fillet-foundation effect is of about 50% difference as compared with each other as shown in fig. (9a). Third, there is large variation between constant Hertzian contact and non-constant Hertzian contact. There are about three times differences between both assumptions of Hertzian contact as shown in Fig. (9b).

Figure 10 presents the relative error of above individual deflection cases. The variable deflection of non-constant Hertzian contact with the various pressure angles and gear tooth types are described in Fig. 11. Figure (11a) describes the influence of the gear mesh stiffness with respect to the various pressure angles and

Fig. (11b) describes the influence of the gear mesh stiffness with respect to the various gear tooth types. The results show that the influence of the deflection by non-constant Hertzian contact obviously depends on gear tooth types. The primary reason is that the strong stub-tooth provides the more normal contact force on the tooth surface. Furthermore, the defections of non-constant Hertzian contact with various gear types are significantly different to those of the various pressure angles. According to above results, the previous models may be overestimated the gear mesh stiffness of a spur gear pair. In other words, the proposed model of this paper can avoid the overestimation problem on the gear mesh stiffness of realistic phenomenon.

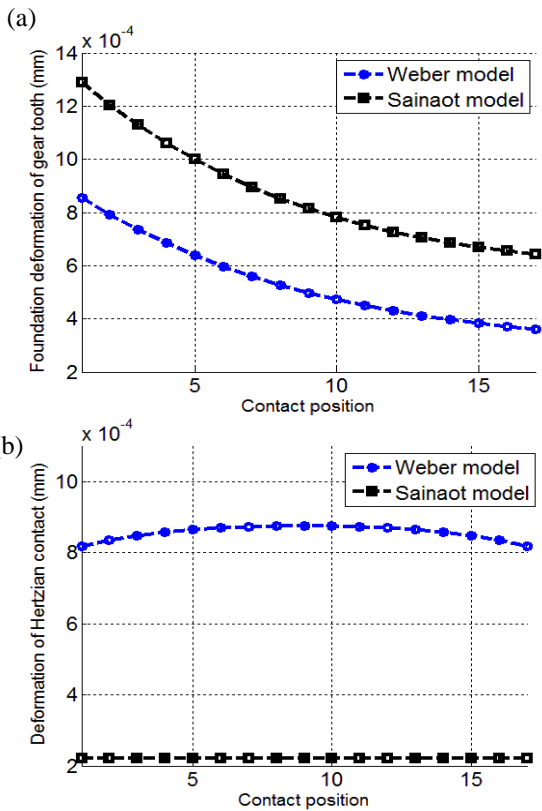


Fig. 9. The comparison of deformation (a) with basic tooth, foundation and (b) Hertzian contact between Weber's model and Sainat's model

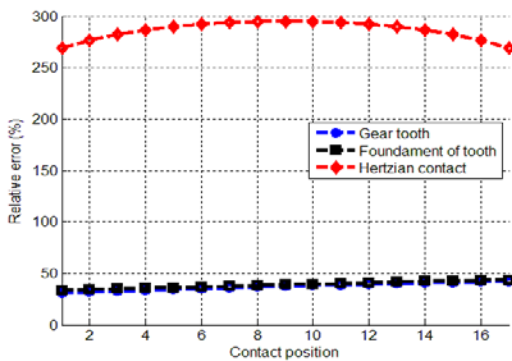


Fig. 10. The variation of the relative error is for gear

tooth, foundation of tooth, and Hertzian contact between Weber's model and Sainat's model.

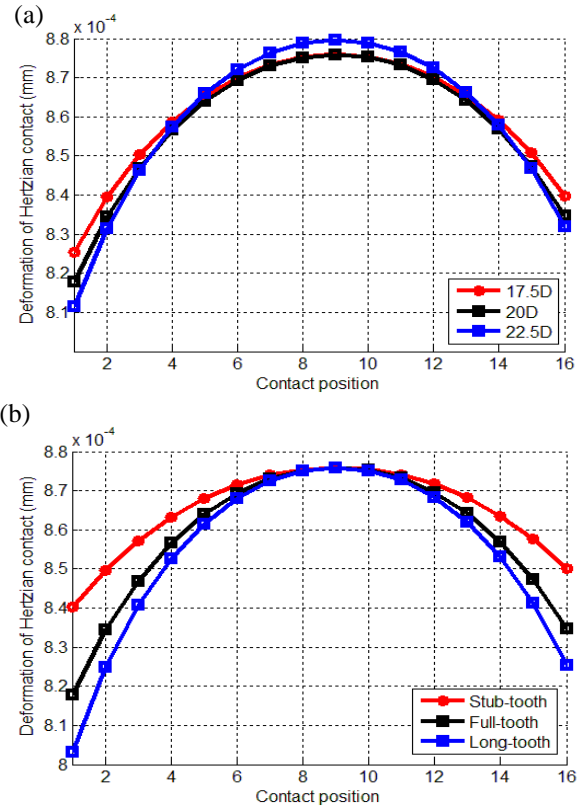
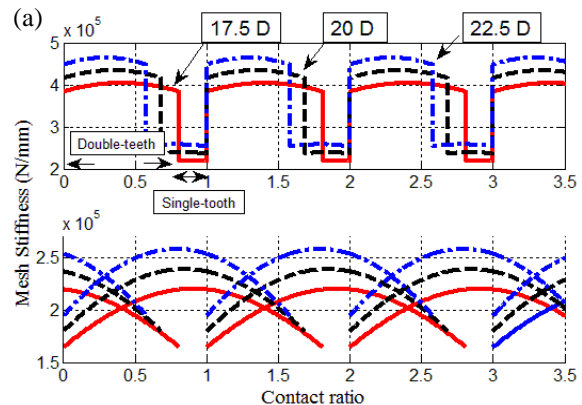


Fig. 11. The comparison of non-constant Hertzian contact with (a) full-tooth with various pressure angles (b) pressure angle of 20 degree with various gear types.

Figure 12 presents the gear mesh stiffness without backlash for various gear parameters. The gear mesh stiffness of the various pressure angles in full-tooth gear type without backlash is illustrated in Fig. (12a). The contact ratios are 1.8107, 1.6836 and 1.5788, which correspond to pressure angles of  $17.5^\circ$ ,  $20^\circ$  and  $22.5^\circ$ , respectively. Figure (12b) shows that the stub-tooth gear pair has the property of higher gear mesh stiffness and lower contact ratio. The long-tooth gear pair has the property of higher contact ratio and lower meshing stiffness. Similarly, the contact ratio of stub-tooth, full-tooth, and long-tooth are 1.3823, 1.6836, and 1.8296, respectively.



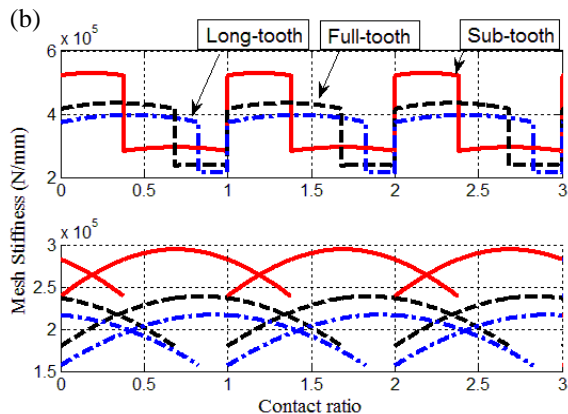


Fig 12. Gear mesh stiffness of proposed model with effect of (a) various pressure angles with the full-tooth type, and (b) various tooth profiles with the pressure angle of 20 degree.

#### 4. Conclusion

An improved model which investigates the advantages of Weber's model and Sinaot's model is proposed to predict the gear mesh stiffness. The effect of circular elastic rings under dedendum circle and non-constant Hertzian contact are employed to calculate the meshing stiffness of a spur gear pair. The numerical results are summarized as follow.

1. The gear mesh stiffness of the proposed model with effect of circular elastic rings under dedendum circle and non-constant Hertzian contact effect is of about 20% difference compared to Weber's model and Sinaot's model.
2. The proposed model can avoid the overestimate problem of gear mesh stiffness by integrating the merits of circular elastic rings under dedendum circle from Sinaot's model and non-constant Hertzian contact from Cornell's model.
3. The variation of gear mesh stiffness for the various gear tooth types under the non-constant Hertzian contact effect will affect the system more than the various pressure angles.

#### References

- A. Kahraman, and G. W. Blankenship, "Interactions between commensurate parametric and forcing excitations in a system with clearance", *Journal of Sound and Vibration*, Vol. 194, No. 3, pp. 317-336 (1996).
- A. Kahraman, and G. W. Blankenship, "Effect of involute contact ratio on spur gear dynamics", *Journal of Mechanical Design*, Vol. 121, pp. 112-118 (1999).
- A. I-shyyab, and A. Kahraman, "Nonlinear dynamic analysis of a multi-mesh gear train using multi-term harmonic balance method: period-one motions", *Journal of Sound and Vibration*, Vol. 284, pp. 151-172 (2005).

- A. Al-shyyab, and A. Kahraman, "Nonlinear dynamic analysis of a multi-mesh gear train using multi-term harmonic balance method: sub-harmonic Motions", *Journal of Sound and Vibration*, Vol. 279, pp. 417-451 (2005).
- C. Weber, "The Deformation of Loaded Gears and The Effect on Their Load-Carrying Capacity", Sponsored Research (Germany), British Dept. of Scientific and Industrial Research, Report No. 3 (1949).
- D. C. H. Yang, and Z. S. Sun, "A rotary model for spur gear dynamics", *Journal of Mechanisms Transmission and Automatic in Design*, Vol. 107, pp. 529-535 (1985).
- F. Chaari, W. Baccar, M. S. Abbes and M. Hadder, "Effect of Spalling or Tooth Breakage on gear mesh stiffness and dynamic response of one-stage spur gear transmission", *European Journal of Mechanics A/Solids*, Vol. 27, pp. 697-705 (2008).
- F. Chaari, T. Fakhfakh and M. Hadder, "Analytical modelling of spur gear tooth crack and influence on gear mesh stiffness", *European Journal of Mechanics A/Solids*, Vol. 28, pp. 461-468 (2009).
- F. L. Litvin, I. Gonzalez-Perez, K. Yukishima, A. Fuentes, and K. Hayasaka, "Generation of planar and helical elliptical gears by application of rack-cutter, hob, and shaper", *Journal of Computer Method in Applied Mechanics Engrg.*, Vol. 196, pp. 4321-4336 (2007).
- F. L. Litvin, A. Fuentes, "Gear Geometry and Applied Theory", second ed., Cambridge University Press (2004).
- H. Ma, R. Z. Song, X. Pang, and B. C. Wen, "Time-vary mesh stiffness calculation of cracked spur gears", *Journal of Engineering Failure Analysis*, Vol. 44, pp. 179-194 (2014).
- J. H. Kuang and Y. T. Yang, "An Estimate of Mesh Stiffness and Load Sharing Ratio of a Spur Gear Pair", *International Power Transmission and Gearing Conference*, Vol. 1, pp.1-9 (1992).
- J. H. Kuang and A. D. Lin, "The effect of tooth wear on the vibration spectrum of spur gear pair", *Journal of Vibration and Acoustic*, Vol. 123, pp.311-317 (2001).
- N. L. Muskhelishvili, "Some Basic Problems of the Mathematical Theory of Elasticity", 2nd English Edition, P. Noordhoff Limited, The Nethrtlands, pp. 230-235 (1975).
- O. D. Mohammed, M.Rantatalo, and J. O. Aidanpaa, "Improving mesh stiffness calculation of cracked gears for the purpose of vibration-based fault analysis", *Journal of Engineering Failure Analysis*, Vol. 34, pp.235-251 (2013).
- P. Sinaot, P. Velez and O. Duverger, "Contribution of Gear Body to Tooth Deflections - A New

Bidimensional Analysis Formula", <i>Journal of Transaction of the ASME</i> , Vol. 126, pp.748-752 (2004).	$b_c$	: Characteristic width
R. W. Cornell, "Compliance and stress sensitivity of spur gear teeth", <i>Journal of Mechanical Design</i> , Vol. 103, pp. 447-459 (1981).	$C$	: Total compliance
R. G. Parker, S. M. Vijayakar, and T. Imajo, "Non-linear dynamic response of a spur gear pair: modelling and experimental comparisons", <i>Journal of Sound and vibration</i> , Vol. 237, pp. 435-455 (2000).	$c_k$	: Clearance
R. Ma, and Y. S. Chen, "Research on the dynamic mechanism of the gear system with local crack and spalling failure", <i>Journal of Engineering Failure Analysis</i> , Vol. 26, pp. 12-20 (2012).	$c_p, c_g$	: displacements of center distance
S. L. Harris, "Dynamic Loads on the Teeth of Gears", <i>Proceedings of the Institution of Mechanical Engineering</i> , Vol. 172, pp. 87-112 (1958).	$E$	: Equivalent elastic modulus
S. L. Chang, C. B. Tsay and L. I. Wu, "Mathematical Model and Undercutting Analysis of Elliptical Gears Generated by Rack cutter", <i>Journal of Mechanism Machine Theory</i> , Vol. 31, No. 7, pp. 879-890 (1994).	$F_L$	: Applied force
S. Theodossiades, and S. Natisavas, "Periodic and chaotic dynamics of motor-driven gear-pair systems with backlash", <i>chaos, Solitons and Fractals</i> , Vol. 12, pp. 2427-2440 (2001).	$h_f$	: Addendum
S. Chen, J. Y. Tang, C. W. Luo, and Q. Wang, "Nonlinear dynamic characteristics of geared rotor bearing systems with dynamic backlash and friction", <i>Journal of Mechanism and Machine Theory</i> , Vol. 46, pp.466-478 (2011).	$I_i$	: Polar mass moment of inertia
Y. Shen, S. Yang, and X. Liu, "Nonlinear dynamics of a spur gear pair with time-varying stiffness and backlash based on incremental harmonic balance method", <i>International Journal of Mechanical Sciences</i> , Vol. 48, No. 11, pp. 1256-1263 (2006).	$I_{A_i}$	: Area moment of inertia
Z. Chen and Y. Shao, "Dynamic simulation of spur gear with tooth root crack propagating along tooth width and crack depth", <i>Journal of Engineering Failure Analysis</i> , Vol. 18, pp. 2149-2164 (2011).	$\vec{i}, \vec{j}, \vec{k}$	: Unit coordinate vector
Z. G Wan, H. R Cao, Y. Y. Zi, W. P. He, and Z. J. He, "An improved time-varying mesh stiffness algorithm and dynamic modeling of gear-rotor system with tooth root crack", <i>Journal of Engineering Failure Analysis</i> , Vol. 42, pp. 157-177 (2014).	$\bar{K}_m$	: Average meshing stiffness of gear pair
	$L_F$	: Effective fillet length
	$[M_{ij}]$	: Transformation matrix
	$\mathbf{N}_i, \mathbf{n}_i$	: Normal vector and unit normal vector
	$\mathbf{n}_p^{(1)}$	: Unit normal vector
	$q$	: Decimal part of contact ratio
	$r_p$	: Radius of pitch circle
	$r_{bi}$	: Radius of base circle
	$r_o$	: Radius of pitch circle
	$r_{op}, r_{og}$	: Radii of pitch circle for gear and pinion
	$\mathbf{r}_1^{(1)}, \mathbf{r}_1^{(2)}$	: Tooth profile vector at fixed coordinate
	$\mathbf{r}_2^{(1)}, \mathbf{r}_2^{(2)}$	: Tooth profile vector at rotating coordinate
	$\mathbf{r}_{fp}^{(1)}$	: Tooth profile vector of pinion
	$\mathbf{r}_{fg}^{(1)}$	: Tooth profile vector of gear
	$s_o$	: Length of contact
	$S_a, S_b$	: Parallel moving coordinates of pinion and gear
	$S_p, S_g, S_F$	: Rotational coordinate of pinion, gear, and fixed coordinate
	$t_e$	: Base pitch
	$t_f$	: Dedendum
	$t_o$	: Standard pitch
	$u_1$	: Straight line section parameter of rack cutter
	$W$	: Tooth width
	$x$	: Modification coefficient
	$x_p, x_g$	: Modification coefficient for pinion and gear, respectively
	$y_T$	: Total deflection of tooth
	$Z_i$	: Number of gear mesh

## NOMENCLATURE

$A_i$	: Cross-section of the $i^{th}$ element
$b$	: Hertz-contact half width
$b_i$	: Backlash of the $i^{th}$ gear pair

Greek symbols

$\alpha$	: Pressure angle
$\alpha_b$	: Mesh pressure angle
$\rho$	: Radius of fillet
$\theta_1$	: Arc section parameter of rack cutter
$\delta_H$	: Hertz contact deflection
$\varepsilon_o$	: Contact length
$\varepsilon_a(\bar{t})$	: Indiscriminate length on contact length
$\phi$	: Rotational angle
$\phi_p, \phi_g$	: Rotational angle of pinion and gear

Subscripts

$F$	: Fixed coordinate
$g, p$	: Gear and pinion
$Fg$	: Rotating coordinate of gear transform to fixed coordinate
$Fp$	: Rotating coordinate of pinion transform to fixed coordinate

---